LIQUID CRYSTALS, 1995, VOL. 19, NO. 2, 159–167

Multifractality of lyotropic liquid crystal formation of aluminium dodecylbenzenesulphonate

by Đ. TEŽAK*, M. MARTINIS† S. PUNČEC, I. FISCHER-PALKOVIĆ, and F. STRAJNAR

Department of Chemistry, Faculty of Science, University of Zagreb, Marulićev trg 19, P.O. Box 163, HR-41001-Zagreb, Croatia

(*Received 17 June 1994; in final form 18 October 1994; accepted 18 December 1994*)

The formation of colloidal and liquid crystalline aggregates of aluminium dodecylbenzenesulphonate caused by mixing aqueous solutions of $Al(NO_3)_3$ and dodecylbenzenesulphonic acid (HDBS) was investigated by light scattering and polarizing microscopy. Applying a fractal approach, some aggregates can be considered as multifractals and some as fractals, depending on the slopes of the '$\lg I(Q)$ versus $\lg Q$' plots (for multifractals the slopes are > 3). A model of multiscaling for the calculation of fractal dimensions in the formation of the liquid crystalline phases is proposed, describing both the spacial and the temporal dependence of amphiphile self-aggregation. The basic symmetries of the dynamics of formation and the structures of the liquid crystalline phases were found to be consistent.

1. Introduction

The formation of Al^{3+} and $Al(OH)_2^+$ compounds with dodecylbenzenesulphonic acid (HDBS) in aqueous solutions under controlled pH conditions was examined. The interaction of aluminium(III) ions with amphiphile (surfactant) molecules in aqueous solution is of considerable interest for a number of reasons such as the involvement of such systems in some disorders in human pathology [1], ecotoxicity in natural waters [2, 3] and adsorption by river sediments [4]; the phase behaviour of the products may, also give an insight into the organization of lipid molecules in general [5, 6]. In a previous study Ilda and Tracey [7] investigated the interaction of $Al(OH)_2^-$ and $Al(OH)_6^{3+}$ complexes with amphiphiles.

2. Experimental

2.1. *Materials*

Dodecylbenzenesulphonic acid (HDBS), a commercial product of 'Ventron', Germany, is an isomeric mixture of normal and branched compounds containing approximately 80 per cent of C_{11} and C_{12}, and 18 per cent of C_9, C_{10}, C_{13}, and C_{14} isomers (by HPLC analysis), and 1·5–2 per cent of unsulphonated material, was used without further purification; a nominal value for the molar concentration, obtained using a value of 326·5 for the weighted mean value of the relative molecular mass was determined by potentiometric titration with NaOH standard solution.

Analytically pure $Al(NO_3)_3 \times 9H_2O$ from 'Kemika', Zagreb, dissolved in water, was standardized gravimetrically with 8-hydroxyquinoline. Dilute nitric acid was used for pH adjustment. Doubly distilled water was used in all experiments.

2.2. *Methods*

Relative turbidity measurements for precipitation diagrams were carried out using a Zeiss tyndallometer connected to a Pulfrich photometer, and using a Virtis Brice Phoenix DU2000 SLS photometer. The methods used for sample preparation and also for the determination of the precipitation diagrams have been described previously [8].

Light scattering measurements were made over a range of scattering angles ($\theta = 5$–$145°$) using an Otsuka SLS photometer. The recording time over the whole range of angles was approximately 2 min. The sampling from each preparation was only done ten times in order to minimize inaccuracy that might be caused by possible settling out of the colloidal dispersion. The scattering volume was 10 cm^3. Before measurements, aqueous solutions were filtered using a 0·22 nm Millipore filter. The light scattering intensity was used to determine the fractal dimension d_f, from the slopes of the straight lines of the log/log plot assuming the power law scattering equation

$$I(Q) \propto Q^{-d_f}. \quad (1)$$

The scattering intensities, $I(Q)$, were plotted as a

* Author for correspondence.

† 'Rugjer Boškovic' Institute, Bijenička c.54, HR-41001-Zagreb, Croatia.

function of the length of the scattering vector, $|\mathbf{Q}| = Q = 4\pi n\lambda^{-1}\sin\theta/2$, (where n is the refractive index, λ is the wavelength of the incident beam, and θ is the scattering angle).

The refractive indices were found to be constant in all samples, i.e. $n = 1{\cdot}337$ for aluminium dodecylbenzenesulphonate in water, and $n = 1{\cdot}345$ for HDBS in water (10–40 wt %).

The particle size distribution obtained using the Otsuka QELS photometer was compared with the distribution patterns determined by means of a Brookhaven BI-200SM QELS photometer, using a BI9000AT Correlator.

The photomicrographs were obtained by using a Leitz Wetzlar optical microscope with polarizing equipment.

2.3. *Interpretation of precipitation data*

The solubility product of Al dodecylbenzenesulphonate was calculated from experimental data obtained at 20°C, and pH = 2·2, using the Debye–Hückel formula for the mean activity coefficient, $y_{\pm}$. When calculating the ionic strength, the effective concentration of nitric acid was also taken into account. According to the equilibrium

$$Al(NO_3)_3(aq) + 3\,HDBS(aq) \rightleftharpoons Al(DBS)_3(s), \quad (2)$$

the apparent solubility product, k_{so}^{app}, is given by the relationship

$$k_{so}^{app} = c(Al^{3+}) \cdot c^3(DBS^-) \cdot y_{\pm}^4. \quad (3)$$

The value of k_{so}^{app} was considered to be a notional mean value since the HDBS is not isometrically pure. It was assumed that the HDBS was completely dissociated [9]. At pH = 2·2, Al^{3+} ion can be considered to be the predominant ionic species in the solution, whereas the mononuclear $Al(OH)_2^+$ ion is predominant at pH = 4·5 [10]. When calculating the concentration of $Al(NO_3)_3$, it was considered that this amounts to practically 100 per cent in solutions at pH = 2·2 [10]. The complicated kinetic behaviour of aluminium ion hydrolysis was not taken into account, and the diluted samples were freshly prepared.

Because of the hydrolysis which occurs in an aluminium nitrate solution at pH = 4·5, by adding HDBS, the following equilibrium can be expected:

$$Al(OH)_2^+ + DBS^- \rightleftharpoons Al(OH)_2DBS(s); \quad (4)$$

The concentration solubility constant can be calculated using the expression

$$k_{so}^{c} = c(Al(OH)_2^+ \cdot C(DBS^-)/mol^2\,dm^{-6}. \quad (5)$$

3. Results and discussion

3.1. *Solubility equilibria*

Precipitation diagrams are presented in figures 1 and 2 in the form of logarithmically plotted molar concentrations of $Al(NO_3)_3$ versus HDBS, in aqueous solutions with and without nitric acid, at estimated pH values of 2·2 and 4·5, respectively. The low concentration domains of reacting components represented homogenous systems of solvated ions in water. These domains are separated from the two phase heterogeneous domains, i.e. from precipitated systems, by solubility limits which represent the borderline with a zero quantity of precipitated phase in solution, and assume that there is a predominance of different simple or complex ions throughout the concentration regions.

The domains I–V are indicated in figure 1. (i) Aqua-complexes in an excess of aluminium nitrate; (ii) The predominance of simple reactant ions due to the low concentrations; the apparent solubility product of $Al(DBS)_3$ (pH = 2·2) calculated from the experimental points on the line with slope 0·33 (see figure 1) determined

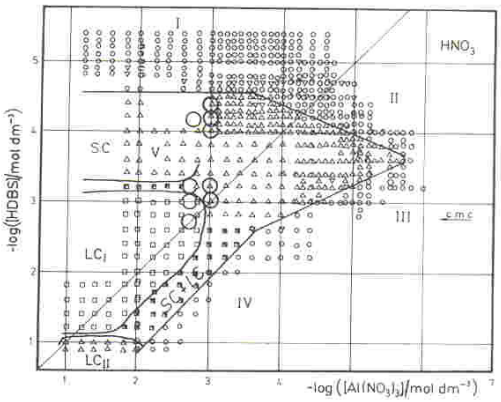

Figure 1. Precipitation diagram of the system $Al(NO_3)_3$/HDBS/H_2O at 20°C; pH is adjusted to 2·2 with dilute HNO_3.

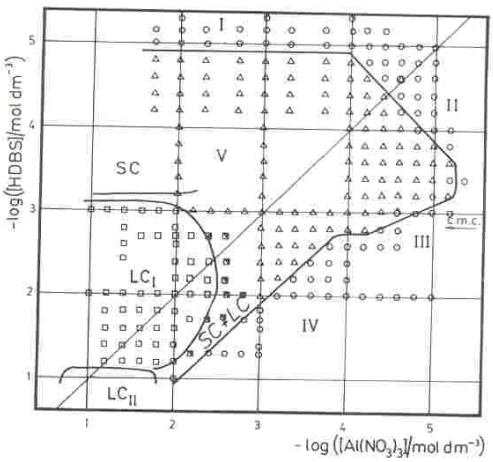

Figure 2. Precipitation diagram of the system $Al(NO_3)_3$/HDBS/H_2O at 20°C; approximately pH = 4·5.

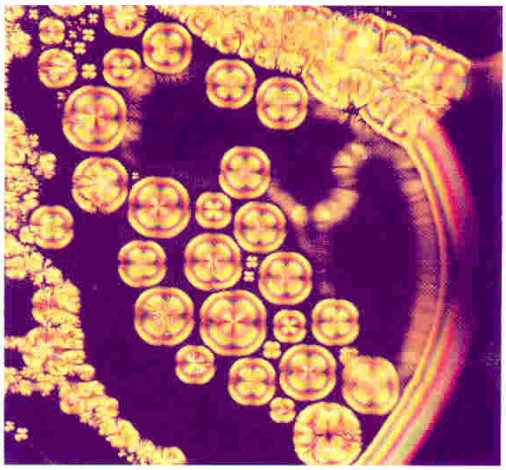

Figure 3. Photomicrograph of the precipitated system with $[Al(NO_3)_3] = 6 \times 10^{-3}$ mol dm^{-3} and [HDBS] = $1{\cdot}5 \times 10^{-2}$ mol dm^{-3}. Crossed polarizers; magnification 250 ×.

(*a*)

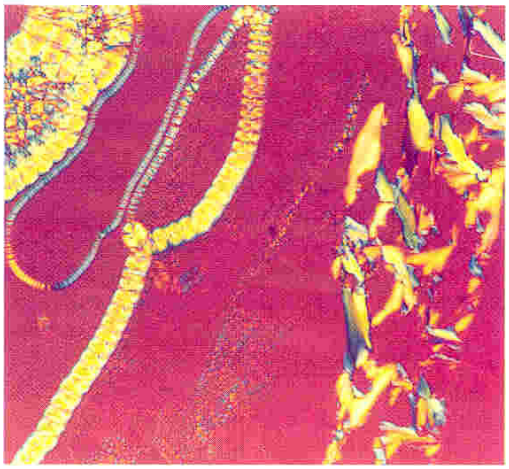

(*b*)

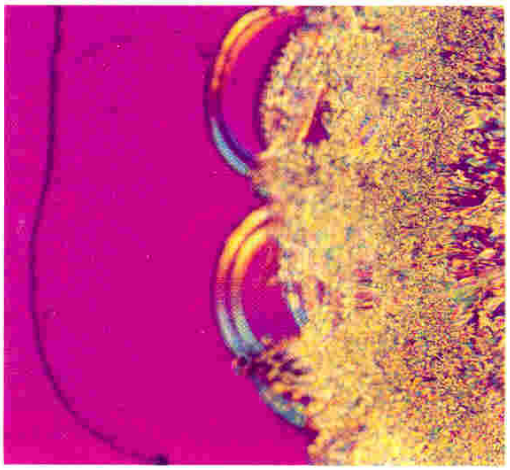

(*c*)

Figure 4. Contact preparations showing the formation of lyotropic mesophases by the mutual penetration of a 10^{-1} molar solution of $Al(NO_3)_3$ (on the right) and the 98 per cent oily HDBS solution (on the left); the phase regions are identified from right to left: (*a*) *Recently prepared sample* (the '$Al(NO_3)_3$ side' of the sample): isotropic phase ($Al(NO_3)_3$ solution); narrow band of nematic or possibly focal-conic structures located at the lamellar isotropic boundary; homeotropic region (pseudo-isotropic); a region of very fast movement of lamellar cylinders folding and becoming spherulites. (*b*) *Sample after 30 min with developed structures* (the same sample as in (*a*)): isotropic phase ($Al(NO_3)_3$ solution; either nematic or developing focal-conic structures; homeotropic; lamellar spherulites of the same size, organized in 'chains'. (*c*) *Recently prepared sample* which remains the same after 30 min, due to the high viscosity (the '98 per cent HDBS side' of the sample): a lamellar/inverse cubic viscous isotropic phase exhibiting curved lines on the left-hand side; on the right, the lamellar tubuli and the fan-shaped lamellar texture. Crossed polarizers 1λ-plate, magnification 80 ×.

to be $k_{so}^{app} = (2{\cdot}25 \pm 0{\cdot}87) \times 10^{-17}$; the concentration solubility product of $Al(OH)_2DBS$ (pH = 4·5) according to the experimental points on the line with slope 0·5 (see figure 2) amounted to $k_{so}^{c} = (9{\cdot}57 \pm 0{\cdot}49) \times 10^{-10}\,mol^2\,dm^{-6}$; (iii) A domain or transition region containing the premicellar aggregates of HDBS [8], limiting the formation of dimers at 2×10^{-4} and the formation of micelles at $1{\cdot}7 \times 10^{-3}\,mol\,dm^{-3}$. Thus this is the region where the formation of premicellar aqua-complexes takes place. These premicellar particles are precursors of micellar complexes in solution; (iv) Above the c.m.c. of a tenzide (surfactant or amphiphile), the micellar complexes are formed in solution. Considering the formation of new phases from the solution, by increasing the concentrations of the reacting components, solid crystalline aggregates are formed in the concentration regions where there is a predominance of simple ions, while the formation of liquid crystalline phases occurs where there is a predominance of premicellar and micellar complexes in the solution; (v) Precipitation regions with the liquid crystalline domains (LC_I) and (LC_{II}) covering the equivalence region above the c.m.c. of HDBS, the solid crystalline domain (SC) in the concentration region of HDBS lower than the c.m.c., and the mixture of the two phases in an excess of HDBS near the solubility limit in equilibrium with the micellar associates in solution. The existence of different hydrated species of aluminium ions can be assumed within the aqueous part of the bilayer of premicellar and micellar phases.

3.2. *Microscopic observations*

Phases separated from a supernatant solution and sedimented to the bottom of test-tubes; some of them, highly viscous with a compact bilayer structure, were removed from the sample, and observed by polarizing microscopy between a slide and a cover slip. The LC_I phase shows characteristic lamellar textures, with spherulites of different sizes and structural regularities, most of which were well organized, exhibiting maltese crosses when viewed between crossed polarizers, while some of them could be considered as structures composed of aggregated small focal-conics consisting of bilayers, presumably with elastic distortions and arbitrary undulated layers, as proposed by Fournier and Durand [11]; some bilayer aggregates forming 'chains' of focal conic aggregates can also be seen in figure 3. Figure 4 (*a*) shows a newly prepared sample of a contact preparation (several seconds); a 10^{-1} molar aqueous solution of $Al(NO_3)_3$ penetrates from the right hand side. The 'cylindrical' separation from the homeotropic phase can be compared with the cylindrical growth of smectic A liquid crystals formed by amphiphilic molecules in dodecyl alcohol [12]. The vertical line of birefringent material on the right hand side can be considered to be either a nematic phase, or a chain of focal-conic units at the lamellar/isotropic boundary. This boundary is temporary and concentration dependent, perhaps indicating a precursor nematic phase.

The LC_{II} is a highly viscous, almost optically isotropic phase (from figures 1 and 2). In addition, the X-ray diffraction experiments showed the existence of two different interplanar distances, i.e. (32·4 ± 0·03) Å for LC_I and 34 Å for LC_{II} phase [13]. According to the X-ray diffraction patterns, both phases are lamellar. The increase in the lamellar distance is presumably caused by bend dislocations of the lamellar planes arising during the transition from the flat lamellar (LC_I) into the curved lamellae of LC_{II}; the phase is very viscous and caused possibly be an inverse cubic phase (there is no optical birefringence). The micrograph in figure 4 (*b*), taken 30 min after the contact preparation was made, presents from the right to left hand side, i.e. with increasing HDBS concentration, isotropic $Al(NO_3)_3$ solution, birefringent features which may be nematic or focal-conic, a homeotropic—presumably nematic or lamellar phase (either of discotic micelles oriented perpendicular to the incident light beam [14], or of flat lamellar layers parallel to the cover slide) containing traces of the focal-conic texture, and the lamellar phase with the well-developed 'chains' of focal-conics. The lamellar/inverse cubic transition can be seen in a contact preparation in figure 4 (*c*) by the penetration of a 10^{-1} molar solution of $Al(NO_3)_3$ into 98 per cent HDBS. From the right to the left hand side, the typical fan-shaped lamellar phase, then a sharp transition to the viscous, optically isotropic inverse cubic phase, can be seen.

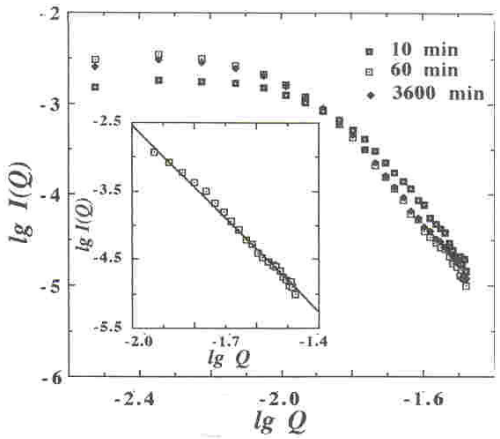

Figure 5. Bilogarithmic plot of intensity of scattered light versus scattering vector for the system prepared from aqueous solutions of $[Al(NO_3)_3] = 2 \times 10^{-3}\,mol\,dm^3$ and $[HDBS] = 6 \times 10^{-4}\,mol\,dm^{-3}$. Inset: the plot of the linear part with a correlation factor amounting to 0·991. The Q-dimension is in Å.

3.3. *Fractal approach*

Microscopic textures, as well as transmission electron micrographs (of freeze fractured and freeze etched preparations) (results to be published) indicated that the formation of self-similar structures (self-similar clusters or aggregates) with defined periodicity, can be assumed to occur in the process of lyotropic liquid crystal formation. Therefore, we have tried to characterize the dynamics and structure of a heterogeneous phase (which happened to be liquid crystalline), formed by mixing a solution of aluminium nitrate with a solution of HDBS, by a fractal approach (the samples denoted by open circles in figure 1). It is clear that mesophase formation may be viewed as a complicated random process that produces structures that are self-similar in the sense that the two-point density–density correlation function

$$C(r) = \frac{1}{N}\int_V d^3Vr', \langle \rho(\mathbf{r}')\rho(\mathbf{r}' + \mathbf{r})\rangle \qquad (6)$$

exhibits scale invariance and is of a power law form, $C(r) \propto r^{d_f - 3}$, where

$$N = \int_V d^3rVC(r).$$

Such structures are known as fractals [15]: their patterns tend to look the same at different levels of resolution (scale length) restricted to those between the limits imposed by the monomer size and the cluster size.

If N is the total number of particles in the fractal aggregate, ρ is the particle density inside the fractal aggregate, r is the inter-particle distance, V is the irradiated volume of the sample, then $C(r)$ represents the interparticle (density–density) correlation function.

In light scattering experiments, the intensity of scattering, $I(Q)$, from a single fractal,

$$I(Q) \propto N\int_V d^3r \exp(i\mathbf{Qr})\, VC(r), \qquad (7)$$

measures the Fourier transform of the density–density correlation function, $C(r)$.

The power law behaviour of the pair correlation function, $C(r)$, is observed as an equivalent power law decay in $I(Q) \propto Q^{-d_f}$ [see equation (1)]. The bilogarithmic plot of the 'intensity of scattered light versus length of the scattering vector' is presented in figure 5 (as an example among many describing the formation of a liquid crystalline phase in a supernatant fluid). A plot of the linear parts of the functions fit lines with slopes greater than 4 with a correlation factor above 0·99 (although the linear parts of a straight line regime fit a power less than one, we tried to do the fractal analysis); all the results are given in table 1. These indicate that the new phase exhibits colloidal character in the early period at the 'short times' (10 min after preparing the sample, and perhaps earlier). Some slopes show values under 3 (see table 1). However, the straight lines with slopes greater than 3 in almost all the samples presented in table 1 fit very well with 'long times' (after 1 h). These values indicate that the formation

Table 1. Slopes and fractal dimensions (d_f) of aluminium dodecylbenzenesulphonate calculated in terms of model (*a*) using equation (12); mean molecular mass of fractal aggregates (M) at time = 3600 min.

Conc./mol dm^{-3}	Slopes			d_f	$2R$/nm	M
Time/min:	10	60	3600		10	3600
$[Al(NO_3)_3]$: 2×10^{-3}						
[HDBS]: 2×10^{-3}	2·59	3·48		2·36	514·4	$9·7\times10^{7}$
1×10^{-3}	4·16	4·55	4·56	3·38	288·1	
6×10^{-4}	4·33	4·53	4·92	1·87	475·1	$1·2\times10^{6}$
2×10^{-4}					430·6	
1×10^{-4}					316·2	
6×10^{-5}		5·16			350·6	
$\eta/cP = 0·891$						
$[Al(NO_3)_3]$: 1×10^{-3}						
[HDBS]: 1×10^{-3}	4·34	4·55	4·79	2·83	167·3	$2·3\times10^{9}$
6×10^{-4}	4·69	4·48			334·7	
2×10^{-4}					416·3	
1×10^{-4}	4·85	5·02	4·69	3·32	397·1	$2·9\times10^{9}$
6×10^{-5}	1·88	6·33			255·4	
4×10^{-5}		3·08	3·36	1·03	241·1	$8·5\times10^{2}$
$\eta/cP = 0·890$						

of lyotropic liquid crystals of alkylbenzenesulphonates can be considered to be a very strictly defined process from the very beginning. The self-ordering of amphiphile molecules can be described in terms of the same mechanism, in the cases of the formation of both crystalline and liquid crystalline phases. This view can be justified by previous X-ray diffraction investigations which showed bilayer and multilayer patterns having the values determined for the interplanar distances in both the SC and LC phases and differing by approximately 1·6 Å [13].

Both, the surfaces and the bulk of the mass can exhibit fractal properties. The magnitude of the power law exponent from a fractal scatterer can show whether the scatterer is a mass or a surface fractal. The magnitude of the exponent is less than 3 for mass fractals, whereas for surface fractals it is $3 < 6 - d_f \leq 4$ [16].

The phenomenon of unexpected high values of the slopes in the 'lg $I(Q)$ versus lg Q' plots shown by lyotropic liquid crystalline phases can be considered in terms of surface fractality or multifractality. The term multifractality implies two or more modes of self-similar aggregation on different scales.

In explaining the non-ideality (or, let us say, not very high precision) of the values of the slopes presented in figure 5 and table 1 for systems measured at different times after sample preparation, it has to be taken into account that there are considerable differences between 'ideal' systems (considering the size, structure, monodispersity or fractality of well-defined colloids like polystyrene latex or colloidal gold [16–19]) and liquid crystalline phases prepared by mixing reacting components and causing the formation of a heterogeneous phase in a supernatant solution. *A different mode of preparation of the latter systems causes differences in the kinetics of formation of the new phase, which can influence the cluster mass distribution in the aggregated particles.* According to Keefer and Schafer [20] and Schmidt [16] there is a possibility of growth of fractally rough colloids, which can be interpreted as surface fractals with exponents approaching 4.

However, two models considering (*a*) the size of the

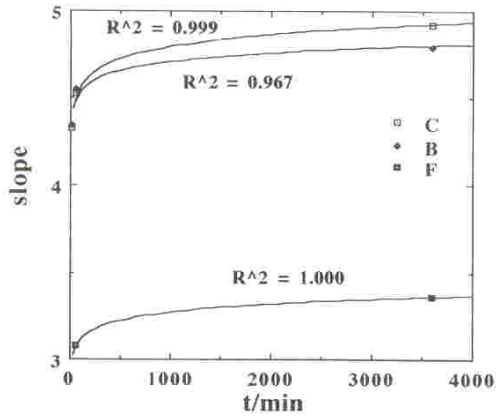

Figure 6. Time dependence of slopes of the plots from figure 5, showing a logarithmic relationship; the correlation factors are indicated.

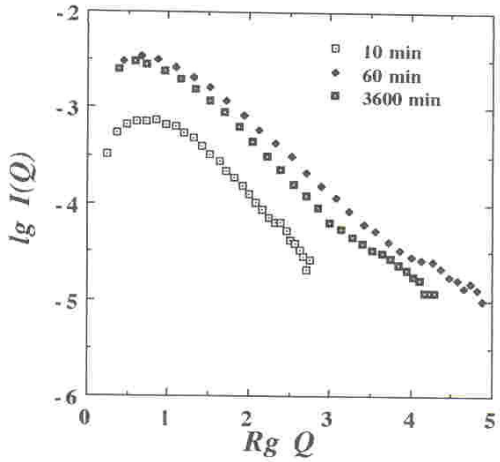

Figure 7. Angular light scattering dependence of gyration radius multiplied by the lengths of the scattering vectors for the system from figure 5.

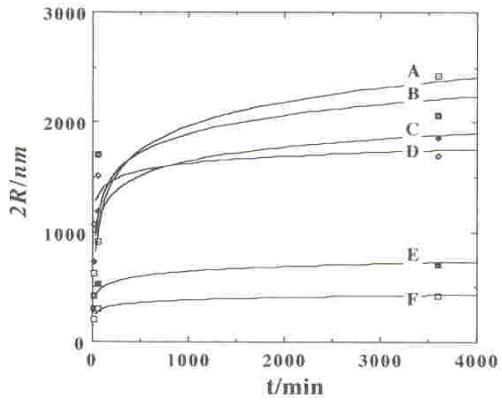

Figure 8. Time-dependence of the average cluster radii (R) showing a logarithmic relationship for the systems prepared from the aqueous solutions containing:

	$[Al(NO_3)_3]$/mol dm^{-3};	[HDBS]/mol dm^{-3};	Correlation factor (R^2)
A	2×10^{-3}	2×10^{-3}	0·997
B	1×10^{-3}	1×10^{-3}	0·736
C	2×10^{-3}	6×10^{-4}	0·989
D	1×10^{-3}	6×10^{-4}	0·798
E	1×10^{-3}	1×10^{-4}	0·915
F	1×10^{-3}	4×10^{-5}	0·979

particles (average cluster radii), and (*b*) the time-dependence of the fractal dimensions, could be proposed in order to explain slopes greater than 3. Generally, the intensity of scattered light, $I(Q)$, from a polydisperse system involves contributions from particles of all sizes. It is, therefore, a function of a radius, R, and a normalized size distribution, N, of particles, and can be written as

$$I(Q) = \int dR\, N(R) I_0(Q, R) = \langle I_0(Q, R) \rangle, \tag{8}$$

with

$$\int dR\, N(R) = 1. \tag{9}$$

The basic assumption is expressed as

$$I_0(Q, R) \to Q^{-d_f(R)}. \tag{10}$$

(a) *Model for* $d_f(R)$ (the fractal dimension is a function of an average cluster radius):

$$d_f(R) = d_f + \beta \ln R + \ldots, \tag{11}$$

$$I(Q) \to \int dR\, N(R) \exp(-d_f(R) \ln Q), \tag{12}$$

$$I(Q) = Q^{-d_f} \int dR\, N(R) \exp(-\beta \ln R \ln Q),$$

$$= Q^{-d_f} \int dR\, N(R) R^{-\beta \ln Q}. \tag{13}$$

If $N(R)$ is narrow,

$$I(Q) \to Q^{-d_f - \beta \ln \bar{R}}, \tag{14}$$

where

$$\bar{R} = \int dR\, RN(R). \tag{15}$$

(b) *Model for* $N(R,t)$

If the particle size distribution is a function of time,

$$\int dR\, RN(R, t) = \bar{R}(t); \tag{16}$$

in the sense that the average value of R is a function of the growth time of the particles or clusters,

$$I(Q) \to \langle Q^{-d_f(R)} \rangle_t; \tag{17}$$

$$I(Q) \to Q^{-d_f(\bar{R}(t))}. \tag{18}$$

The fractal dimensions for liquid crystalline phases of Al dodecylbenzenesulphonate, calculated applying equation (12), are presented in table 1. From the values achieved (mainly under 3, and some of them greater than 3, which would come from the surface fractal character of the process), the multifractality of these samples can be explained in terms of multiscaling. It is obvious that it depends on particle sizes, following the exponential function as in equation (12). The basic symmetry of the dynamics of formation and structure of liquid crystals was found to be consistent, i.e. it is self-similar, but multifractal in terms of time. The slopes in figure 5, are constant with time, but this is true for one-scaling regime: the time-dependence of the slopes presented in figure 6 shows that there is one scaling related to the first aggregation time period ('short times'), while the system is going through the colloidal state (slopes under 3), and the other ('long times'), while the slopes reach the constant values.

Self-similarity is confirmed quite convincingly by the presentation of scattering intensities with gyration radii in figure 7, i.e. the statistical distribution in the regime $R_g Q \ll 1$, the transition regime for $R_g Q = 1$, and a well-defined structure symmetry in the regime $R_g Q \gg 1$.

The average molecular mass of fractal aggregates, M which scales with the size, R, defined as $M \sim R^{d_f}$ ([17] and reference [3] therein), is presented in table 1 for the long aggregation time period (3600 min), showing high values (these values are correspondingly smaller for the first aggregation periods).

Concerning model (*b*), it is obvious from figure 8, that the average cluster radii increase with aggregation time on the logarithmic scale, approaching a limiting value.

The comparison of the Gaussian mass distribution of the aggregated particles within the nematic regime was made at the times of 10 min and 1 d after the sample preparation,

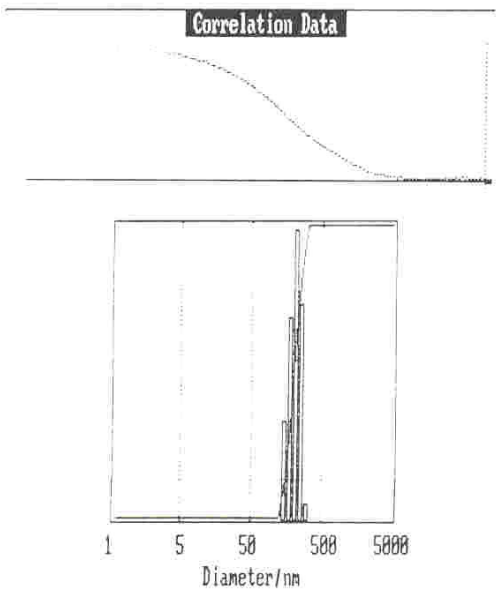

Figure 9. Intensity distribution versus diameter of aggregated particles for the sample of Al dodecylbenzenesulphonate in water from results obtained using the B19000AT Correlator, 3600 min after preparation. Molar concentrations of the reacting components were: $Al[NO_3)_3 = 2 \times 10^{-3}$, $HDBS = 1 \times 10^{-3}$; mean cluster diameter 1901 nm.

Table 2. Mean diameters of fractal aggregates as they change with time; every sample was prepared separately; measurements were performed using both the Otsuka and Brookhaven QELS photometer.

Sample and conc./mol dm^3	Time/min	$2R$/nm	
		Otsuka	Brookhaven
$Al(NO_3)_3 = 2 \times 10^{-3}$/HDBS $= 1 \times 10^{-3}$	10	288·1	263
	3600	1736·1	1901
$Al(NO_3)_3 = 1 \times 10^{-3}$/HDBS $= 1 \times 10^{-3}$	10	167·3	
	3600	2058·3	1448
$Al(NO_3)_3 = 1 \times 10^{-3}$/HDBS $= 1 \times 10^{-4}$	10	397·1	
	3600	708·7	184 and 620 (bimodal)

Table 3. Slopes (some of which can be considered fractal dimensions) of different phases appearing in HDBS/H_2O solutions at 20°C.

HDBS/H_2O(w/w%)	Slope	R^2†	Phase‡	η/cP	D_{diff}/cm^2 s^{-1}§	$2R$/nm	d_f
10	non-fractal		I_l	0·896	$8{\cdot}57 \times 10^{-10}$	5690·4	
20	1·384	0·993	I_h	0·890	$2{\cdot}97 \times 10^{-7}$	16·5	1·38
30	1·367	0·995	I_h				1·37
32	3·127	0·996	I/N	0·899	$5{\cdot}28 \times 10^{-6}$	0·9	
34	5·136	0·996	N	0·895	$3{\cdot}72 \times 10^{-6}$	1·3	
36	5·920	0·997	N	0·907	$6{\cdot}17 \times 10^{-6}$	0·8	
38	6·130	0·996	N				
40	1·648	0·997	L				1·65

† R^2 is the correlation factor; the reliability of slope determination for the I_h phase is lower than for the more defined phases in the sense of fractality.

‡ I_l = isotropic, low viscosity; I_h = isotropic, high viscosity (premicellar), I/N = isotropic to nematic (transition), N = nematic, L = lamellar.

§ Diffusion coeffcients (D_{diff}) and average cluster radii (R) show rather unreliable values because of bubbles.

using both, the Otsuka and Brookhaven QELS photometers. Taking into account that the systems are polydisperse, and that the way of mixing samples constitutes an imperfect step (i.e. the samples have been independently mixed for each experiment, and could show different aggregation kinetics), the distribution in the chosen samples presented in figure 9 and table 2 can be considered quite reliable; the clusters formed after 1 d with higher values of the mean diameters show the narrower size distribution.

The measurements performed both on the Otsuka or Brookhaven instrument showed good agreement. The fractal dimensions remain the same after some critical initial period of time, as shown in table 1. The precision of the mean particle mass determination is within 20 per cent.

3.4. *Indication of phase transition using the fractal approach*

The results of the determination of slopes in the lg $I(Q)$ versus lg Q plot indicate that the transition between

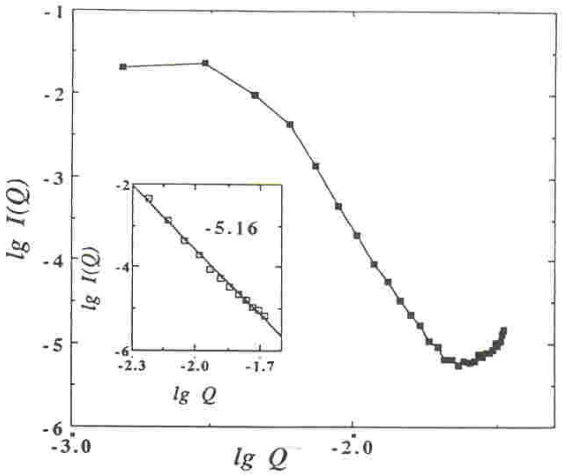

Figure 10. Bilogarithmic plot of intensity of scattered light versus length of scattering vector for the 'HDBS/H_2O(w/w 34 per cent)' sample. Inset: the plot of the linear part exhibiting the slope − 5·16 and having a correlation factor of 0·996. The Q-dimension is in Å.

different liquid crystalline phases can be predicted with high reliability. The slopes were determined for samples which had been chosen using the phase diagram of the 'HDBS/H_2O' system from ref [14], and are presented in table 3. It is obvious that the low viscosity isotropic phase (I_l) is not fractal, premicellar phases (I_h) show a loose cluster mass distribution ($d_f = 1{\cdot}375$), the slope for isotropic/nematic phase transition (I/N) shows a value over 3, while the slopes indicating a nematic phase (N) approach values of 6; the slope for this sample of a lamellar phase (L) can be considered as $d_f = 1{\cdot}65$, if we assume that this loose cluster mass distribution presents a fractality on the non-variable scale. The angular scattering plot in figure 10 for the lyotropic nematic 'HDBS/H_2O' sample shows that it can be characterized as a fractal. It is however an open question if the multifractality of this nematic can be explained in terms of variant fractal scaling.

The authors are grateful to the Ministry of Science and Technology of the Republic of Croatia for the financial support for this scientific investigation.

References

[1] ILDA, M., and TRACEY, A. S., 1991, *Langmuir*, **7,** 202.
[2] CRONAN, C. S., 1990, *Environ. Sci. Technol.*, **24,** 1100.
[3] WILHELM, M., JÄGER, D. E., and OHNESORGE, K., 1990, *Pharmacology, Toxicology*, **66,** 4.
[4] MARCHESI, J. R., HOUSE, W. A., WHITE, G. F., RUSSELL, N. J., and FARR, I. S., 1991, *Coll. Surf.*, **53,** 63.
[5] TANFORD, C., 1978, *Science*, **200,** 1012.
[6] STEWARD, G. T., 1966, *Molec. Crystals liq. Crystals*, **1,** 563.
[7] ILDA, M., and TRACEY, A. S., 1990, *J. phys. Chem.*, **94,** 2590.
[8] TEŽAK, Đ., STRAJNAR, F., ŠARČEVIĆ, D., MILAT, O., and STUBIČAR, M., 1984, *Croat. Chem. Acta*, **57,** 93, including reference [14] therein.
[9] TEŽAK, Đ., ČOLIĆ, M., HRUST, V., POPOVIĆ, S., PRGOMET, S., and STRAJNAR, F., 1987, *Progr. Coll. polym. Sci.*, **74,** 87.
[10] BAES, C. F., and MESMER, R. E., 1976, *The Hydrolysis of Cations* (Wiley Interscience, New York).
[11] FOURNIER, J. B., and DURAND, G., 1991, *J. Phys. II France*, **1,** 845.
[12] PRATIBHA, R., and MADHUSUDANA, N. V., 1992, *J. Phys. II France*, **2,** 383.
[13] TEŽAK, Đ., POPOVIĆ, S., HEIMER, S., and STRAJNAR, F., 1989, *Progr. Coll. Inter. Sci.*, **79,** 293.
[14] TEŽAK, Đ., HERTEL, G., and HOFFMANN, H., 1991, *Liq. Crystals*, **10,** 15.
[15] MARTIN, J. E., and HURD, A. J., 1987, *J. appl. Cryst.*, **20,** 61.
[16] SCHMIDT, P. W., 1990, *The Fractal Approach to Heterogeneous Chemistry*, edited by D. Avnir (Wiley, Chichester), p. 67–79.
[17] KLEIN, R., WEITZ, D. A., LIN, M. I., LINDSAY, H. M., BALL, R. C., and MEAKIN, P., 1990, *Progr. Coll. polym. Sci.*, **81,** 161.
[18] PFEIFER, P., AVNIR, D., and FARIN, D., 1991, *Large Scale Molecular Systems—Quantum and Stochastic Aspects*, edited by W. Gans, A. Blumen, and A. Amann (NATO ASI Series B, Plenum, New York), p. 215–229.
[19] ASNAGHI, D., CARPINETI, M., GIGLIO, M., and SOZZI, M., 1992, *Progr. Coll. polym. Sci.*, **89,** 60.
[20] KEEFER, K. D., and SCHAEFER, D. W., 1986, *Phys. Rev. Lett.*, **56,** 2376.